minerals

MDPI

Article

Jahn-Teller Distortion and Cation Ordering: The Crystal Structure of Paratooite-(La), a Superstructure of Carbocernaite

Sergey V. Krivovichev [1,2,*], Taras L. Panikorovskii [2,3], Andrey A. Zolotarev [2], Vladimir N. Bocharov [4], Anatoly V. Kasatkin [5] and Radek Škoda [6]

1 Nanomaterials Research Centre, Kola Science Centre, Russian Academy of Sciences, Fersmana 14, 184209 Apatity, Russia
2 Department of Crystallography, Institute of Earth Sciences, St. Petersburg State University, University Emb. 7/9, 199034 St. Petersburg, Russia; taras.panikorovsky@spbu.ru (T.L.P.); aazolotarev@gmail.com (A.A.Z.)
3 Laboratory of Nature-Inspired Technologies and Environmental Safety of the Arctic, Kola Science Centre, Russian Academy of Sciences, Fersmana 14, 184209 Apatity, Russia
4 Geo Environmental Centre "Geomodel", Saint-Petersburg State University, Ul'yanovskaya Str. 1, 198504 St. Petersburg, Russia; bocharov@molsp.phys.spbu.ru
5 Fersman Mineralogical Museum, Russian Academy of Sciences, Leninsky Prospekt 18-2, 119071 Moscow, Russia; anatoly.kasatkin@gmail.com
6 Department of Geological Sciences, Faculty of Science, Masaryk University, Kotlářská 2, 61137 Brno, Czech Republic; rskoda@sci.muni.cz
* Correspondence: s.krivovichev@ksc.ru; Tel.: +7-81555-7-53-50

Received: 23 May 2019; Accepted: 18 June 2019; Published: 20 June 2019

Abstract: The crystal structure of paratooite-(La) has been solved using crystals from the type locality, Paratoo copper mine, near Yunta, Olary Province, South Australia, Australia. The mineral is orthorhombic, *Pbam*, $a = 7.2250(3)$ Å, $b = 12.7626(5)$ Å, $c = 10.0559(4)$ Å, $V = 927.25(6)$ Å^3, and $R_1 = 0.063$ for 1299 unique observed reflections. The crystal structure contains eight symmetrically independent cation sites. The *La* site, which accommodates rare earth elements (REEs), but also contains Sr and Ca, has a tenfold coordination by seven carbonate groups. The Ca, Na1, and Na2 sites are coordinated by eight, eight, and six O atoms, respectively, forming distorted CaO_8 and $Na1O_8$ cubes, and Na_2O_6 octahedra. The Cu site is occupied solely by copper and possess a distorted octahedral coordination with four short (1.941 Å) and two longer (2.676 Å) apical Cu–O bonds. There are three symmetrically independent carbonate groups $(CO_3)^{2-}$ with the average <C–O> bond lengths equal to 1.279, 1.280, and 1.279 Å for the C1, C2, and C3 sites, respectively. The crystal structure of paratooite-(La) can be described as a strongly distorted body-centered lattice formed by metal cations with $(CO_3)^{2-}$ groups filling its interstices. According to the chemical and crystal-structure data, the crystal-chemical formula of paratooite-(La) can be described as $(La_{0.74}Ca_{0.11}Sr_{0.07})_4CuCa(Na_{0.75}Ca_{0.15})(Na_{0.63})(CO_3)_8$ or $REE_{2.96}Ca_{1.59}Na_{1.38}CuSr_{0.28}(CO_3)_8$. The idealized formula can be written as $(La,Sr,Ca)_4CuCa(Na,Ca)_2(CO_3)_8$. The structure of paratooite is a $1 \times 2 \times 2$ superstructure of carbocernaite, $CaSr(CO_3)_2$. The superstructure arises due to the ordering of the chemically different Cu^{2+} cations, on one hand, and Na^+ and Ca^{2+} cations, on the other hand. The formation of a superstructure due to the cation ordering in paratooite-(La) compared to carbocernaite results in the multiple increase of structural complexity per unit cell. Therefore, paratooite-(La) versus carbocernaite represents a good example of structural complexity increasing due to the increasing chemical complexity controlled by different electronic properties of mineral-forming chemical elements (transitional versus alkali and alkaline earth metals).

Keywords: paratooite-(La); crystal structure; carbonate; carbocernaite; superstructure; rare earth elements; copper; cation array; cation ordering; archetype

1. Introduction

Rare earth elements (REE)-bearing carbonates belong to one of the most widespread group of REE minerals and are the major form of the REE occurrence at the largest world mineral deposits such as Bayan Obo, China [1,2]. REE carbonate minerals also show a large range of chemical and structural variations, which is reflected in the recent discoveries and investigations [3–12]. In addition, inorganic REE carbonates are important from the material science point of view, showing interesting physical and chemical properties [13–17].

There are very few natural REE carbonates containing transitional metals such as copper. Only four Cu-REE carbonate minerals are known to date: schuilingite-(Nd), $CuPbNd(CO_3)_3(OH)\cdot 1.5H_2O$ [18–20], astrocyanite-(Ce), $Cu_2Ce_2(UO_2)(CO_3)_5(OH)_2\cdot 1.5H_2O$ [21], decrespignyite-(Y), $Y_4Cu(CO_3)_4Cl(OH)_5\cdot 2H_2O$ [22], and paratooite-(La), $(La,REE,Ca,Na,Sr)_6Cu(CO_3)_8$ or $REE_3(Ca,Sr)_2NaCu(CO_3)_8$ (according to the original description [23], see below). Both decrespignyite-(Y) and paratooite-(La) have been found in the Paratoo copper deposit near Yunta, South Australia, Australia. The assemblage of rare earth minerals at this locality is associated with the weathered base metal and magnetite ores. The origin of paratooite-(La) is due to the secondary hydrothermal reworking of primary ores, where REEs and copper were introduced by hydrothermal fluids [24]. Paratooite-(La) forms tiny crystals, thin and flexible, which prevented the structural characterization of the species up to date. Pring et al. [23] tried to solve the crystal structure from the high-resolution synchrotron powder data, but their attempts were unsuccessful.

The aim of the present paper is to report on crystal structure of paratooite-(La) solved using single crystal from the type locality, and to describe its structural correlations with related phases.

2. Materials and Methods

2.1. Materials

The specimen of paratooite-(La) studied herein originates from its type locality, Paratoo copper mine, near Yunta, Olary Province, South Australia, Australia. It comes from the collection of one of us (A.V.K.) and was obtained in 2007 from the senior author of the original description of the species Dr. Allan Pring (South Australian Museum, Adelaide, Australia). Paratooite-(La) occurs as pale blue radiating aggregates on matrix and associates with bastnäsite-(La), donnayite-(Y), kamphaugite-(Y), malachite, and nontronite. Individual crystals are tabular and reach up to $60 \times 40 \times 10$ μm^3 in size.

2.2. Chemical Composition

The chemical composition of the mineral was studied by scanning electron microscopy and electron-probe microanalysis using both ED and WD spectrometers. Preliminary semi-quantitative chemical analysis was made in the laboratory of the Fersman Mineralogical Museum (Moscow, Russia) using a CamScan 4D SEM equipped with an ED spectrometer and INCA Energy microanalyzer (conditions of analysis: Accelerating voltage 20 kV, beam current 5 nA on metallic cobalt, and beam diameter 5 μm).

Quantitative chemical composition of paratooite-(La) was conducted in the laboratory of electron microscopy and microanalysis at the department of geological sciences, Masaryk University (Brno, Czech Republic), using a Cameca SX 100 electron probe at WDS mode (conditions of analysis: Accelerating voltage 15 kV, beam current 10 nA, beam diameter 5 μm, and impulses time acquisition at peak—10 s for main elements and 20–120 s for minor elements). The following standards were used: NaK_α—albite A; CaK_α—wollastonite; SrL_α—$SrSO_4$; BaL_α—baryte; CuK_α—lammerite; YL_α—YAG; LaL_α—$LaPO_4$; PrL_β—$PrPO_4$; NdL_β—$NdPO_4$; SmL_β—$SmPO_4$; GdL_β—$GdPO_4$; and SiK_α—andalusite.

The average chemical composition was as follows (in wt. %): Na_2O 4.33, CaO 8.35, SrO 2.51, BaO 0.03, CuO 5.86, Y_2O_3 0.57, La_2O_3 24.85, Pr_2O_3 2.18, Nd_2O_3 7.65, Sm_2O_3 0.63, Gd_2O_3 0.50, SiO_2 0.46, CO_2 (calc.) 28.30, and total 86.22. Paratooite forms porous aggregates composed of very thin crystals. Due to the sensitivity of the mineral to an electron beam, the mineral was analyzed under

defocused conditions (10 μm in diameter) to reduce the electron-beam flux density, which resulted in the low analytical total. The empirical chemical formula calculated on the basis of C + Si = 8 and O = 24 (as in the original study [23]) can be written as $Na_{1.72}Sr_{0.30}Ca_{1.84}Cu_{0.91}La_{1.88}Nd_{0.56}Pr_{0.16}Y_{0.06}Sm_{0.04}Gd_{0.03}C_{7.91}Si_{0.09}O_{24}$. This agrees generally well with the chemical formula defined in [23] as $Na_{1.16}Sr_{0.33}Ca_{1.47}Cu_{0.79}La_{1.77}Nd_{0.53}Pr_{0.57}Y_{0.07}Sm_{0.04}Gd_{0.05}C_{7.92}N_{0.27}$- $O_{23.87}F_{0.12}$, taking into account the difficulties associated with the rapid deterioration of crystals under the electron beam. Both chemical formulae are also in general agreement with the results of crystal-structure study (see below).

2.3. Single-Crystal X-ray Diffraction Study

A single-crystal X-ray diffraction study of paratooite-(La) was performed at the Resource Center "X-ray Diffraction Methods" of St. Petersburg State University using a Bruker Kappa APEX DUO diffractometer operated at 45 kV and 0.6 mA and equipped with a CCD area detector. The study was done by means of a monochromatic Mo$K\alpha$ X-radiation (λ = 0.71073 Å), frame widths of 0.5° in ω, and 100 s counting time for each frame. The intensity data were reduced and corrected for Lorentz, polarization, and background effects using the Bruker software APEX2 [25]. A semiempirical absorption-correction based upon the intensities of equivalent reflections was applied (SADABS [26]). The unit cell parameters obtained in this study (Table 1) are in agreement with those reported in the original study [23] (a = 7.2360 Å, b = 12.8088 Å, and c = 10.0862 Å), taking into account the interchange of crystallographic axes for a standard setting. The structure was solved and refined in the space group *Pbam* to R_1 = 0.063 (wR_2 = 0.170) for 1299 unique observed reflections using the ShelX program package [27]. During the refinement, 93 reflections were noticed that violated the absence conditions for the space group *Pbam*. However, all attempts to refine the structure in the lower-symmetry groups resulted in physically unrealistic displacement parameters for C and O atoms and instability of the refinement. In our opinion, the appearance of the "forbidden" reflections may be due to the presence in the crystal studied of ordered domains with lower symmetry, since the structure contains several sites with mixed occupancies and defects (see below). The assignment of cations to the mixed-occupied sites was done on the basis of crystal-chemical considerations and chemical data. Crystal data, data collection, and structure refinement details are given in Table 1; atom coordinates and bond-valence sums (calculated using bond-valence parameters taken from [28]) in Table 2; observed and theoretical site-scattering factors for cation sites in Table 3; anisotropic displacement parameters in Table 4; and selected interatomic distances in Table 5. Supplementary crystallographic data have been deposited as the crystallographic information file (CIF) available at the journal website.

2.4. Raman Spectroscopy

The Raman spectrum of paratooite-(La) single plate crystal was measured using a Jobin–Yvon LabRam HR 800 spectrometer (Horiba, Kyoto, Japan) with a 514 nm laser. The laser beam (2 μm in diameter) was oriented along the c axis. The power at the sample surface was 5–6 mW.

3. Results

3.1. Raman Spectroscopy

The Raman spectrum of paratooite-(La) (Figure 1) agrees well with the previously reported data [23], except for the presence of weak bands in the range from 3200 to 3700 cm^{-1}. These bands are assignable to O–H stretching vibrations, but it is highly unlikely that the crystal structure of paratooite-(La) contains hydroxyl groups as structural elements. There are no sites that could accommodate OH-groups, except for the O sites of the carbonate groups. However, the Raman spectrum does not contain any other bands that could be explained by the presence of bicarbonate groups, $(HCO_3)^-$. It seems most probable that the bands observed at 3460 and 3572 cm^{-1} are artefacts appearing due to the admixture of other minerals or the presence of defects (probably, on the surface of the mineral grain) associated with irregularly distributed protonated O sites.

The most intense band at 1095 and two weak bands at 1369 and 1434 cm^{-1} (Table 6) can be assigned to the C–O symmetric and asymmetric modes of stretching vibrations of the $(CO_3)^{2-}$ groups. The weak bands observed in the range of 900–600 cm^{-1} can be related to the asymmetric and symmetric bending vibrations of the same bonds [29,30]. Only one peak was observed in the region of v_1 vibrations in the $(CO_3)^{2-}$ groups instead of two observed previously (at 1095 and 1075 cm^{-1}), most probably due to the absence of polarization of carbonate groups along the *c* direction [23]. The bands at 386, 343, and 261 cm^{-1} correspond to the bending/stretching vibrations of the Cu–O bonds of the CuO_6 distorted polyhedra [31]. The bands below 150 cm^{-1} can be assigned to the lattice vibrations.

Table 1. Crystal data and structure refinement for paratooite-(La).

Crystal System	Orthorhombic
Space group	*Pbam*
a, Å	7.2250(3)
b, Å	12.7626(5)
c, Å	10.0559(4)
V, $Å^3$	927.25(6)
Z	1
ρ_{calc}, g/cm^3	3.690
μ, mm^{-1}	7.837
Crystal dimensions, mm	0.06 × 0.04 × 0.01
λ, Å	0.71073
2θ range, deg.	4.05–57.92
Index ranges	$-9 \le h \le 7$, $-17 \le k \le 16$, $-13 \le l \le 13$
Reflections collected	9442
Independent reflections	1299 [R_{int} = 0.061]
Data/restraints/parameters	1299/0/111
GOF (goodness-of-fit)	1.103
Final *R* indexes [$I \ge 2\sigma(I)$]	R_1 = 0.063, wR_2 = 0.170
Final *R* indexes (all data)	R_1 = 0.076, wR_2 = 0.195

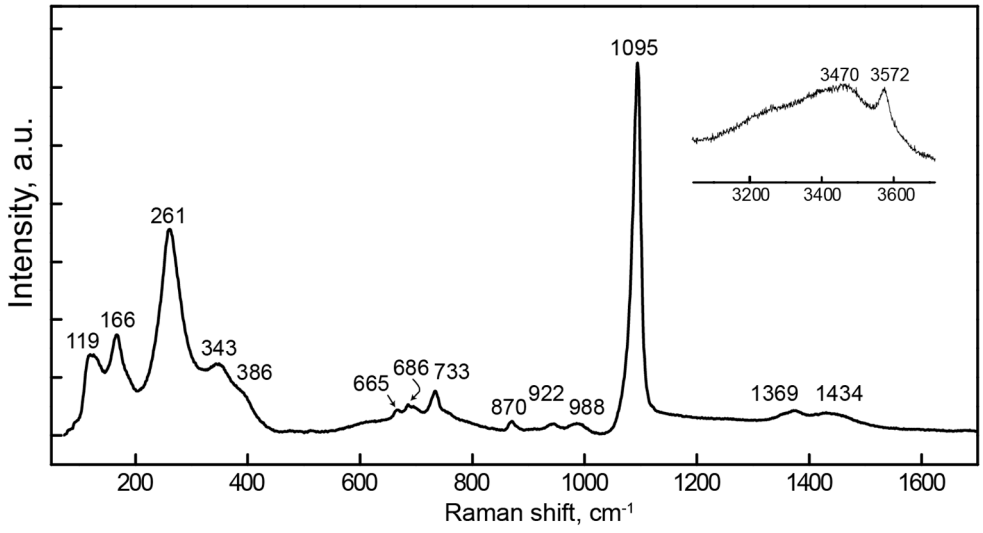

Figure 1. Raman spectrum of paratooite-(La).

3.2. Cation Coordination

The crystal structure of paratooite-(La) contains eight symmetrically independent cation sites (Figure 2). The *La* site, which accommodates REEs, but also contains Sr and Ca, has a tenfold coordination from seven carbonate groups. The Ca, Na1, and Na2 sites are coordinated by eight, eight, and six O atoms, respectively, forming distorted CaO_8 and $Na1O_8$ cubes, and Na_2O_6 octahedra. The Cu site is occupied solely by copper and possesses a distorted octahedral coordination with four short

(1.941 Å) and two longer (2.676 Å) apical Cu–O bonds. This type of distortion is typical for octahedrally coordinated Cu^{2+} ions, according to the well-known Jahn–Teller theorem [32,33]. The crystal structure contains three symmetrically independent C sites that form carbonate groups $(CO_3)^{2-}$ with the average <C–O> bond lengths equal to 1.279, 1.280, and 1.279 Å for the C1, C2, and C3 sites, respectively.

Table 2. Atomic coordinates, isotropic displacement parameters (Å^2), and bond-valence sums (BVS, in valence units (v.u.)) for paratooite-(La).

Atom	*x*	*Y*	*z*	$U_{eq.}$	BVS
La	0.71419(8)	0.69022(5)	0.74855(4)	0.0161(3)	3.31
Cu	$\frac{1}{2}$	$\frac{1}{2}$	$\frac{1}{2}$	0.0222(6)	2.08
Ca	$\frac{1}{2}$	0	0	0.0237(8)	2.07
Na1	0	$\frac{1}{2}$	$\frac{1}{2}$	0.025(2)	1.09
Na2	$\frac{1}{2}$	$\frac{1}{2}$	0	0.017(4)	0.98
C1	0.3107(12)	0.5452(7)	0.7449(6)	0.0159(16)	4.05
C2	0.5435(15)	0.7731(9)	0	0.016(2)	4.04
C3	Vladimir N. Bocharov 0.0438(16)	0.7177(9)	$\frac{1}{2}$	0.017(2)	4.05
O1	0.3047(9)	0.4929(5)	0.6323(6)	0.0233(13)	2.14
O2	0.6306(16)	0.6864(7)	0	0.028(2)	2.11
O3	0.0059(9)	0.6741(5)	0.6122(6)	0.0208(12)	2.11
O4	0.5057(10)	0.8179(4)	0.8891(6)	0.0215(13)	2.18
O5	0.3789(9)	0.6359(5)	0.7497(5)	0.0210(13)	2.19
O6	0.1304(15)	0.8036(7)	$\frac{1}{2}$	0.026(2)	2.14
O7	0.2460(10)	0.4974(6)	0.8447(6)	0.0282(14)	2.22

Table 3. Observed (exp.) and theoretical (theor.) site-scattering factors (SSF, e^-) and assigned occupancies for selected atom sites in the crystal structure of paratooite-(La).

Atom	$SSF_{exp.}$	SSF_{theor}	Occupancy
La	46.64	46.07	$La_{0.71}Sr_{0.10}\square_{0.10}Ca_{0.09}$
Cu	29.00	29.00	Cu
Ca	20.00	20.00	Ca
Na1	11.00	10.62	$Na_{0.82}\square_{0.10}Ca_{0.08}$
Na2	6.38	6.38	$Na_{0.58}\square_{0.42}$

Table 4. Anisotropic displacement atom parameters for paratooite-(La) (Å^2).

Atom	U^{11}	U^{22}	U^{33}	U^{23}	U^{13}	U^{12}
La	0.0247(5)	0.0146(4)	0.0090(4)	−0.00037(18)	−0.00006(19)	−0.00050(19)
Cu	0.0247(5)	0.0146(4)	0.0090(4)	−0.00037(18)	−0.00006(19)	−0.00050(19)
Ca	0.0318(11)	0.0265(12)	0.0083(9)	0	0	0.0026(10)
Na1	0.0347(18)	0.0234(17)	0.0131(14)	0	0	0.0008(16)
Na2	0.038(4)	0.020(4)	0.015(3)	0	0	−0.005(3)
C1	0.016(5)	0.021(6)	0.014(6)	0	0	0.002(5)
C2	0.026(4)	0.014(4)	0.008(4)	−0.003(2)	0.004(3)	0.002(3)
C3	0.024(6)	0.016(5)	0.008(4)	0	0	0.000(4)
O1	0.026(6)	0.018(5)	0.006(4)	0	0	0.001(4)
O2	0.040(3)	0.019(3)	0.011(3)	−0.003(2)	−0.002(2)	0.001(3)
O3	0.045(6)	0.025(5)	0.014(4)	0	0	0.013(4)
O4	0.026(3)	0.020(3)	0.016(3)	0.006(2)	0.003(3)	0.001(3)
O5	0.028(3)	0.019(3)	0.017(3)	0.007(2)	0.000(3)	0.000(2)
O6	0.026(3)	0.017(3)	0.019(3)	0.001(2)	−0.002(2)	−0.005(2)
O7	0.040(5)	0.022(5)	0.015(4)	0	0	−0.010(4)

3.3. Structure Description

The crystal structure of paratooite-(La) is shown in Figure 3a. It can conveniently be described in terms of packing of cations with $(CO_3)^{2-}$ groups filling its interstices. The Ca, Cu, Na1, and Na2

sites locate exactly in the corners of a primitive orthorhombic cell with all unit-cell parameters twice as small as the original cell. The La sites are located in each of the eight subcells that constitute the unit cell, shifting from the centers of the subcells in the *ab* plane along the *b* axis. Therefore, the whole cation array in paratooite-(La) may be considered as a strongly distorted cation-ordered body-centered lattice.

Figure 3 compares the crystal structure of paratooite-(La) (Figure 3a) with that of carbocernaite, ideally $CaSr(CO_3)_2$ [34–38]. It is obvious that the two crystal structures are very similar, with that of paratooite being the superstructure of carbocernaite. The relations between the two structures can be described using the following equations (crb = carbocernaite; prt = paratooite-(La)):

$$a_{prt} = c_{crb} \quad (1)$$

$$b_{prt} = 2b_{crb}, \quad (2)$$

$$c_{prt} = 2a_{crb} \quad (3)$$

Thus, the structure of paratooite-(La) is a $1 \times 2 \times 2$ superstructure of that of carbocernaite. Figure 4 shows the cation packing in paratooite-(La) (a) and its sections at the $z = \frac{1}{2}$ (b) and $z = 0$ (c) levels. This clearly shows that the superstructure arises due to the ordering of the chemically different Cu^{2+} cations, on one hand, and Na^+ and Ca^{2+} cations, on the other hand. The chemical difference arises due to the Jahn–Teller distortion of the Cu^{2+} coordination geometry in contrast to the relatively uniform (in terms of bond lengths) Na^+ and Ca^{2+} coordinations. Thus, one may speculate that the superstructure formation is governed by different electronic properties of cations constituting the crystal structure of paratooite-(La).

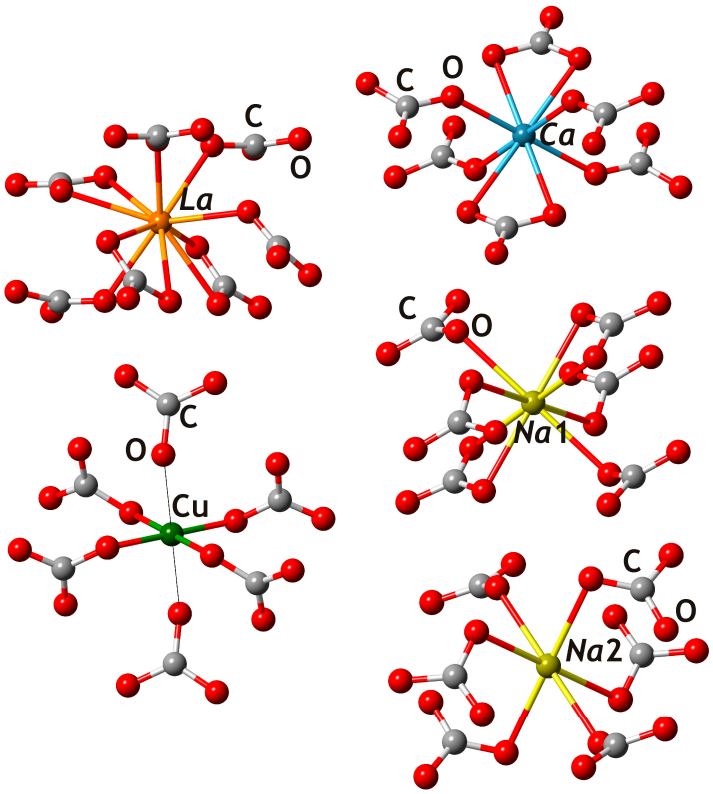

Figure 2. Coordination environments of the La, Ca, Cu, Na1, and Na2 sites in the crystal structure of paratooite-(La). Legend: La, Ca, Na, C, and O atoms are shown as orange, blue, greenish-yellow, gray, and red spheres, respectively.

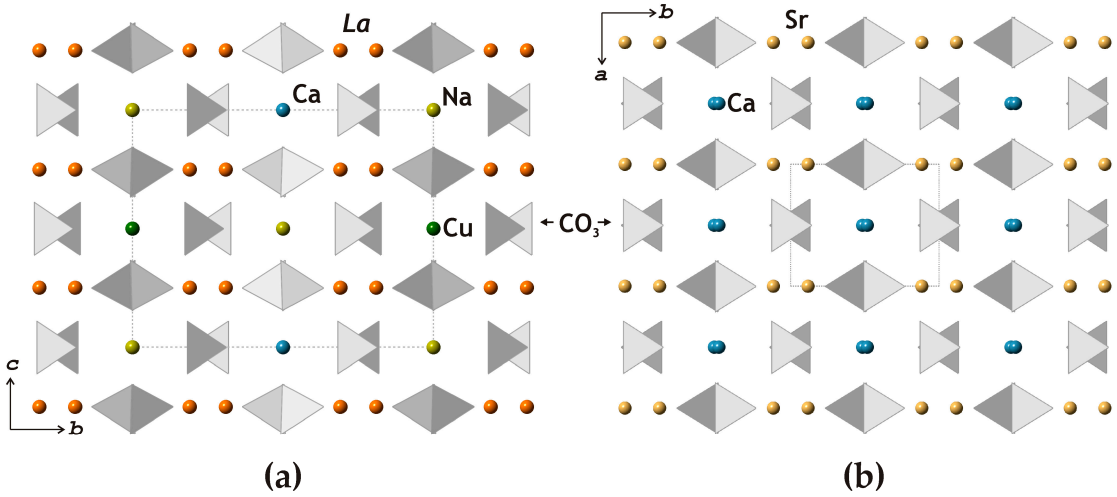

Figure 3. The crystal structures of paratooite-(La) (**a**) and carbocernaite (**b**). Legend is as in Figure 1; Sr atoms are shown as yellow spheres, and carbonate triangles are shaded in gray.

3.4. Crystal-Chemical Formula

According to the chemical and crystal-structure data, the crystal-chemical formula of paratooite-(La) can be described as $(La_{0.74}Ca_{0.11}Sr_{0.07})_4CuCa(Na_{0.75}Ca_{0.15})(Na_{0.63})(CO_3)_8$ or $REE_{2.96}Ca_{1.59}Na_{1.38}CuSr_{0.28}(CO_3)_8$. The idealized formula can be written as $(La,Sr,Ca)_4CuCa(Na,Ca)_2(CO_3)_8$. This formula is in general agreement with the results of chemical analyses reported in the original study [23] and in our work, taking into account the difficulties related with the instability of the mineral under the electron beam.

Table 5. Selected bond lengths (Å) in the crystal structure of paratooite-(La).

La–O5	2.518(7)	Cu–O1	1.941(6) 4×	C1–O5	1.259(11)
La–O5	2.520(7)	Cu–O6	2.676(6) 2×	C1–O7	1.264(9)
La–O3	2.523(6)	<Cu–O>	2.186	C1–O1	1.315(9)
La–O4	2.539(7)			<C1–O>	1.279
La–O6	2.573(3)	Ca–O7	2.367(7) 4x		
La–O7	2.598(7)	Ca–O4	2.578(6) 4x	C2–O2	1.273(14)
La–O2	2.600(3)	<Ca–O>	2.473	C2–O4	1.283(8)
La–O1	2.617(7)			C2–O4	1.283(8)
La–O4	2.631(6)	Na1–O3	2.492(6) 4x	<C2–O>	1.280
La–O3	2.673(6)	Na1–O1	2.573(6) 4x		
<La–O>	2.579	<Na1–O>	2.533	C3–O6	1.262(14)
				C3–O3	1.287(8)
		Na2–O7	2.410(7) 4x	C3–O3	1.287(8)
		Na2–O2	2.560(10) 2x	<C3–O>	1.279
		<Na2–O>	2.460		

Table 6. Raman bands in the paratooite-(La) spectrum and their interpretation.

Raman Shift, cm^{-1}	Assignment	Type
1369 w, 1434 w	CO_3	v_3
1095 s, 988 w *, 922 w *	CO_3	v_1
870 w	CO_3	v_2
733, 686 w, 665 w	CO_3	v_4
386 sh, 343	CuO_6	v_1, v_2
261 s	CuO_6	v_3, v_4
166, 119		lattice vibrations

sh = shoulder; s = strong intensity; w = weak; * these can also be assigned to a small admixture of silicate anions.

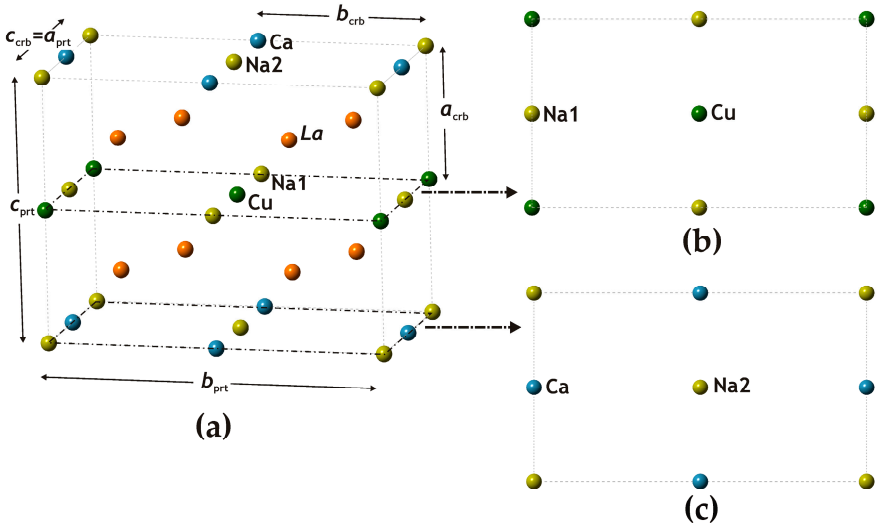

Figure 4. The cation arrangement in the unit cell of the crystal structure of paratooite-(La) (**a**) and its sections on the levels $z = \frac{1}{2}$ (**b**) and 0 (**c**).

4. Discussion

Carbocernaite, ideally $CaSr(CO_3)_2$, was discovered by Bulakh et al. [34] at the Vuoriyarvi complex, Northern Karelia, Russia. Recently, Chakhmouradian et al. [38] investigated carbocernaite from Bear Lodge, Wyoming, USA, and demonstrated that the mineral can be described as a solid solution between $CaSr(CO_3)_2$ and $NaREE(CO_3)_2$. The crystal structure of carbocernaite was originally solved by Voronkov and Pyatenko [36] in the space group $Pb2_1m$, which was confirmed in [37]. However, the recent study of carbocernaite from Wyoming [38] revealed the presence of reflections that violated the above-mentioned space group, very similar to our observations concerning paratooite-(La) (see above). Therefore, the alternative space group was chosen as $P11m$ (Table 6). Our attempts to refine the crystal structure of paratooite-(La) in this space group were unsuccessful, due to the high number of correlations between the displacement parameters of symmetry-related sites. The additional reflections may appear due to the presence of domains with different symmetries or incommensurate modulations induced by complex substitution mechanisms.

The information-based structural complexity parameters have been calculated by means of the TOPOS software [39] using techniques proposed in [40,41] and are listed in Table 7. The formation of a superstructure due to the cation ordering in paratooite-(La) compared to carbocernaite results in the essential increase of structural complexity per unit cell. Therefore, paratooite-(La) versus carbocernaite represents a good example of structural complexity increasing due to the increasing chemical complexity controlled by different electronic properties of mineral-forming chemical elements (transitional versus alkali and alkaline earth metals).

Our study may also have interesting implications with regard to the propensity of the carbocernaite structure type to incorporate chemical elements with drastically different electronic properties. For instance, paratooite-(La) incorporates REE and copper simultaneously, which may be of interest from the viewpoint of its physical properties and, in particular, of its magnetism. However, the experimental study of magnetic and other properties of paratooite-(La) is currently impossible due to the tiny amount of available material. Therefore, it is of interest to reproduce the mineral under laboratory conditions, which would allow to investigate its structure and properties in more details.

Table 7. Unit-cell parameters, space groups, and structural complexity parameters for paratooite-(La) and carbocernaite.

Mineral	Space Group	*a* (Å)	*b* (Å)	*c* (Å)/γ (deg.)	I_G (bits/atom)	$I_{G,total}$ (bits/cell)	
paratooite-(La)	*Pbam*	7.225	12.763	10.056	3.722	297.754	this work
carbocernaite	$P2_1am$ *	7.30	6.41	5.23	2.922	58.439	[36]
carbocernaite	$P2_1am$ *	7.301	6.430	5.214	2.922	58.439	[37]
carbocernaite	$P11m$ *	7.266	6.434	5.220/89.98	3.922	78.439	[38]

* Crystallographic axes interchanged for the ease of comparison.

Supplementary Materials: The following are available online at http://www.mdpi.com/2075-163X/9/6/370/s1, Crystallographic Information File (CIF).

Author Contributions: Conceptualization, T.L.P. and S.V.K.; methodology, T.L.P., V.N.B. and A.V.K.; investigation, T.L.P., A.A.Z., V.N.B., A.V.K. and R.Š.; writing—original draft preparation, S.V.K., T.L.P. and A.V.K.; writing—review and editing, S.V.K., T.L.P. and A.V.K.; and visualization, S.V.K. and T.L.P.

Funding: This research was funded by the Russian Science Foundation (grant 19-17-00038 to S.V.K.).

Acknowledgments: We are grateful to Nikita V. Chukanov for useful comments on the interpretation of the Raman spectrum of paratooite-(La).

Conflicts of Interest: The authors declare no conflict of interest.

References

1. Zhang, P.; Tao, K.; Yang, Z.; Yang, X.; Song, R. Rare earth, niobium and tantalum minerals in Bayan Obo ore deposit and discussion on their genesis. *J. Rare Earths* **2002**, *20*, 81–86.
2. Deng, M.; Xu, C.; Song, W.; Tang, H.; Liu, Y.; Zhang, Q.; Zhou, Y.; Feng, M.; Wei, C. REE mineralization in the Bayan Obo deposit, China: Evidence from mineral paragenesis. *Ore Geol. Rev.* **2017**, *91*, 100–109. [CrossRef]
3. Srinivasan, S.G.; Shivaramaiah, R.; Kent, P.R.C.; Stack, A.G.; Navrotsky, A.; Riman, R.; Anderko, A.; Bryantsev, V.S. Crystal structures, surface stability, and water adsorption energies of La-Bastnäsite via density functional theory and experimental studies. *J. Phys. Chem. C* **2016**, *120*, 16767–16781. [CrossRef]
4. Plášil, J.; Škoda, R. Crystal structure of the (REE)–uranyl carbonate mineral shabaite-(Nd). *J. Geosci.* **2017**, *62*, 97–105. [CrossRef]
5. Ciobanu, C.L.; Kontonikas-Charos, A.; Slattery, A.; Cook, N.J.; Wade, B.P.; Ehrig, K. Short-Range Stacking Disorder in Mixed-Layer Compounds: A HAADF STEM Study of Bastnäsite-Parisite Intergrowths. *Minerals* **2017**, *7*, 227. [CrossRef]
6. Plášil, J.; Petříček, V. Crystal structure of the (*REE*)-uranyl carbonate mineral kamotoite-(Y). *Mineral. Mag.* **2017**, *81*, 653–660. [CrossRef]
7. Schmandt, D.S.; Cook, N.J.; Ciobanu, C.L.; Ehrig, K.; Wade, B.P.; Gilbert, S.; Kamenetsky, V.S. Rare Earth Element Fluorocarbonate Minerals from the Olympic Dam Cu-U-Au-Ag Deposit, South Australia. *Minerals* **2017**, *7*, 202. [CrossRef]
8. Panikorovskii, T.L.; Kalashnikova, G.O.; Zhitova, E.S.; Pakhomovsky, Y.A.; Bocharov, V.N.; Yakovenchuk, V.N.; Zolotarev, A.A.; Krivovichev, S.V. Crystal chemistry of Na-rich kihlmanite-(Ce) from arfvedsonite-aegirine-microcline pegmatite at the Kihlman Mt. (Khibiny massif, Kola Peninsula, Russia). *Zap. Ross. Mineral. Obshch.* **2017**, *146*, 113–124. (In Russian)
9. Kalatha, S.; Perraki, M.; Economou-Eliopoulos, M.; Mitsis, I. On the Origin of Bastnaesite-(La,Nd,Y) in the Nissi (Patitira) Bauxite Laterite Deposit, Lokris, Greece. *Minerals* **2017**, *7*, 45. [CrossRef]
10. Kim, P.; Anderko, A.; Navrotsky, A.; Riman, R.E. Trends in Structure and Thermodynamic Properties of Normal Rare Earth Carbonates and Rare Earth Hydroxycarbonates. *Minerals* **2018**, *8*, 106. [CrossRef]
11. Škoda, R.; Plášil, J.; Čopjaková, R.; Novák, M.; Jonsson, E.; Galiová, M.V.; Holtstam, D. Gadolinite-(Nd), a new member of the gadolinite supergroup from Fe-REE deposits of Bastnäs-type, Sweden. *Mineral. Mag.* **2018**, *82*, 133–145. [CrossRef]

12. Menezes Filho, L.A.D.; Chaves, M.L.S.C.; Chukanov, N.V.; Atencio, D.; Scholz, R.; Pekov, I.; Da Costa, G.M.; Morrison, S.M.; Andrade, M.B.; Freitas, E.T.F.; et al. Parisite-(La), ideally $CaLa_2(CO_3)_3F_2$, a new mineral from Novo Horizonte, Bahia, Brazil. *Mineral. Mag.* **2018**, *82*, 133–144. [CrossRef]
13. Luo, M.; Ye, N.; Zou, G.; Lin, C.; Cheng, W. $Na_8Lu_2(CO_3)_6F_2$ and $Na_3Lu(CO_3)_2F_2$: Rare earth fluoride carbonates as deep-UV nonlinear optical materials. *Chem. Mater.* **2013**, *25*, 3147–3153. [CrossRef]
14. Wang, Y.; Han, T.; Ding, Y.-S.; Zheng, Z.; Zheng, Y.-Z. Sodalite-like rare-earth carbonates: A study of structural transformation and diluted magnetism. *Dalton Trans.* **2016**, *45*, 1103–1110. [CrossRef] [PubMed]
15. Zhang, R.-H.; Zhao, D.; Huang, M.; Yang, R.-J.; Ma, F.-X.; Fan, Y.-C. Synthesis, crystal structure and photoluminescence properties of a new rare-earth carbonate $Na_3Eu(CO_3)_3{\cdot}6H_2O$. *J. Chil. Chem. Soc.* **2017**, *62*, 3403–3406. [CrossRef]
16. Hämmer, M.; Höppe, H.A. Crystalline orthorhombic $Ln[CO_3][OH]$ (Ln = La, Pr, Nd, Sm, Eu, Gd) compounds hydrothermally synthesised with CO_2 from air as carbonate source. *Z. Naturforsch.* **2019**, *74b*, 59–70. [CrossRef]
17. Cao, L.; Song, Y.; Peng, G.; Luo, M.; Yang, Y.; Lin, C.-S.; Zhao, D.; Xu, F.; Lin, Z.; Ye, N. Refractive index modulates second-harmonic responses in $RE_8O(CO_3)_3(OH)_{15}X$ (*RE* = Y, Lu; X = Cl, Br): Rare-earth halide carbonates as ultraviolet nonlinear optical materials. *Chem. Mater.* **2019**, *31*, 2130–2137. [CrossRef]
18. Piret, P.; Deliens, M. Nouvelles données sur la schuilingite, carbonate hydrate de terres rares, de plomb et de cuivre. *Bull. Mineral.* **1982**, *105*, 225–228.
19. Sarp, H.; Bertrand, J.; Deferne, J. Données nouvelles sur la schuilingite de Shinkolobwe (Shaba, Zaire), carbonate hydrate de plomb, cuivre et de terres rares. *Schweiz. Mineral. Petrogr. Mitt.* **1983**, *63*, 1–6.
20. Schindler, M.; Hawthorne, F.C. The crystal structure of schuilingite-(Nd). *Can. Mineral.* **1999**, *37*, 1463–1470.
21. Deliens, M.; Piret, P. L'astrocyanite-(Ce), $Cu_2(TR)_2(UO_2)(CO_3)_5(OH)_2{\cdot}1{,}5\ H_2O$, nouvelle espèce minérale de Kamoto, Shaba, Zaïre. *Eur. J. Mineral.* **1990**, *2*, 407–411. [CrossRef]
22. Wallwork, K.; Kolitsch, U.; Pring, A.; Nasdala, L. Decrespignyite-(Y), a new copper yttrium rare earth carbonate chloride hydrate from Paratoo, South Australia. *Mineral. Mag.* **2002**, *66*, 181–188. [CrossRef]
23. Pring, A.; Wallwork, K.; Brugger, J.; Kolitsch, U. Paratooite-(La), a new lanthanum-dominant rare-earth copper carbonate from Paratoo, South Australia. *Mineral. Mag.* **2006**, *70*, 131–138. [CrossRef]
24. Brugger, J.; Ogierman, J.; Pring, A.; Waldron, H.; Kolitsch, U. Origin of the secondary *REE*-minerals at the Paratoo copper deposit near Yunta, South Australia. *Mineral. Mag.* **2006**, *70*, 609–627. [CrossRef]
25. Bruker-AXS. *APEX2*, Version 2014.11-0; Bruker-AXS: Madison, WI, USA, 2014.
26. Sheldrick, G.M. *SADABS*; University of Goettingen: Goettingen, Germany, 2007.
27. Sheldrick, G.M. Crystal structure refinement with *SHELXL*. *Acta Crystallogr.* **2015**, *C71*, 3–8.
28. Gagné, O.C.; Hawthorne, F.C. Comprehensive derivation of bond-valence parameters for ion pairs involving oxygen. *Acta Crystallogr.* **2015**, *B71*, 562–578. [CrossRef] [PubMed]
29. Frost, R.L.; Martens, W.N.; Rintoul, L.; Mahmutagic, E.; Kloprogge, J.T. Raman spectroscopic study of azurite and malachite at 298 and 77 K. *J. Raman Spectrosc.* **2002**, *33*, 252–259. [CrossRef]
30. Michiba, K.; Miyawaki, R.; Minakawa, T.; Terad, Y.; Nakai, I.; Matsubara, S. Crystal structure of hydroxylbastnäsite-(Ce) from Kamihouri, Miyazaki Prefecture, Japan. *J. Miner. Petrol. Sci.* **2013**, *108*, 326–334. [CrossRef]
31. Buzgar, N.; Apopei, A.I. The Raman study of certain carbonates. *Geologie Tomul L* **2009**, *55*, 97–112.
32. Jahn, H.A.; Teller, E. Stability of polyatomic molecules in degenerate electronic states. I. Orbital degeneracy. *Proc. R. Soc.* **1937**, *A161*, 220–235.
33. Hathaway, B.J. Copper. In *Comprehensive Coordination Chemistry*; Wilkinson, G., Ed.; Pergamon: Oxford, UK, 1987; Volume 5, pp. 533–774.
34. Bulakh, A.G.; Kondrateva, V.V.; Baranova, E.N. Carbocernaite—a new rare-earth carbonate. *Zap. Vses. Mineral. Obsh.* **1961**, *90*, 42–49. (In Russian)
35. Bulakh, A.G.; Izokh, E.P. New data on carbocernaite. *Dokl. Akad. Nauk SSSR* **1967**, *175*, 175–177. (In Russian)
36. Voronkov, A.A.; Pyatenko, Y.A. Crystal structure of carbocernaite $(Na,Ca)(TR,Sr,Ca,Ba)(CO_3)_2$. *J. Struct. Chem.* **1967**, *8*, 835–840. [CrossRef]
37. Shi, N.; Ma, Z.; Peng, Z. The crystal structure of carbocernaite. *Kexue Tongbao* **1982**, *27*, 76–80. (In Chinese)
38. Chakhmouradian, A.R.; Cooper, M.A.; Reguir, E.P.; Moore, M.A. Carbocernaite from Bear Lodge, Wyoming: Crystal chemistry, paragenesis, and rare-earth fractionation on a microscale. *Am. Mineral.* **2017**, *102*, 1340–1352. [CrossRef]

39. Blatov, V.A.; Shevchenko, A.P.; Proserpio, D.M. Applied topological analysis of crystal structures with the program package ToposPro. *Cryst. Growth. Des.* **2014**, *14*, 3576–3586. [CrossRef]
40. Krivovichev, S.V. Structural complexity of minerals: Information storage and processing in the mineral world. *Miner Mag.* **2013**, *77*, 275–326. [CrossRef]
41. Krivovichev, S.V. Which inorganic structures are the most complex? *Angew. Chem. Int. Ed.* **2014**, *53*, 654–661. [CrossRef]